JACS
JOURNAL OF THE AMERICAN CHEMICAL SOCIETY
Article
pubs.acs.org/JACS

Computational Study and Molecular Orbital Analysis of NMR Shielding, Spin−Spin Coupling, and Electric Field Gradients of Azido Platinum Complexes

Kiplangat Sutter and Jochen Autschbach*

Department of Chemistry, State University of New York at Buffalo, Buffalo, New York 14260-3000, United States

Supporting Information

ABSTRACT: ^{195}Pt, ^{14}N, and ^{15}N NMR data for five azido (N_3^-) complexes are studied using relativistic density functional theory (DFT). Good agreement with experiment is obtained for Pt and N chemical shifts as well as Pt−N *J*-coupling constants. Calculated ^{14}N electric field gradients (EFGs) reflect experimentally observed trends for the line broadening of azido ^{14}N NMR signals. A localized molecular orbital analysis of the nitrogen EFGs and chemical shifts is performed to explain some interesting trends seen experimentally and in the first-principles calculations: (i) ^{14}N NMR signals for the Pt-coordinating (N_α) nuclei in the azido ligands are much broader than for the central (N_β) or terminal (N_γ) atoms. The N_β signals are particularly narrow; (ii) compared to N_γ, the N_α nuclei are particularly strongly shielded; (iii) N_β nuclei have much larger chemical shifts than N_α and N_γ ; and (iv) The Pt−N_α *J*-coupling constants are small in magnitude when considering the formal sp hybridization of N_α . It is found that for N_α a significant shielding reduction due to formation of the dative N_α−Pt bond is counterbalanced by an increased shielding from spin−orbit (SO) coupling originating at Pt. Upon coordination, the strongly delocalized π system of free azide localizes somewhat on N_β and N_γ . This effect, along with rehybridization at N_α upon bond formation with Pt, is shown to cause a deshielding of N_γ relative to N_α and a strong increase of the EFG at N_α . The large 2p character of the azide σ bonds is responsible for the particularly high N_β chemical shifts. The nitrogen s-character of the Pt−N_α bond is low, which is the reason for the small *J*-coupling. Similar bonding situations are likely to be found in azide complexes with other transition metals.

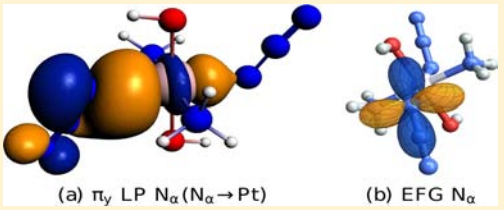

1. INTRODUCTION

There is significant interest in platinum azide complexes due to their potential as photoactivatable anticancer prodrugs.[1,2] The development of platinum-based antitumor agents is aimed at increasing selectivity and lowering the toxicity associated with antitumor drugs. For instance, photoactivatable anticancer agents are supposed to treat localized tumors in a less invasive manner than traditional chemotherapy.[3] A possible mechanism of action is that six-coordinate Pt(IV) complexes get photo-reduced to cytotoxic Pt(II) species upon irradiation.[4] There is also continuing research interest focusing on trans-isomers of platinum complexes, although, unlike cisplatin, transplatin is not active as an antitumor agent.[5−7] However, upon substitution of the transplatin amine ligands with bulky N-donor ligands it was found that the compounds have some potency to inhibit the growth of tumor cells. Mechanistically, it has been hypothesized that the substituted ligands slow down the substitution of the two chlorides in transplatin, thereby improving the kinetic stability of transplatin compounds.[8]

The spin-1/2 ^{195}Pt nucleus has a wide NMR resonance window spanning well over 10 000 ppm.[9,10] Platinum NMR spectroscopy data have been useful in diverse research areas, including cancer research[11] and kinetic studies[12,13] as well as studies of biosensors and biomarkers.[14] ^{195}Pt chemical shifts are sensitive to the nature of the ligands in the coordination sphere of the Pt atom and vary considerably with the oxidation state of the metal.[15] Metal−ligand interactions can play out in subtle ways as they influence the sensitive Pt magnetic shielding. For instance, a ligand may donate electron density to the Pt atom via a dative σ bond (L → Pt) which increases the electron density at the metal, but if there is strong π back donation (L ← Pt), the electron density may be reduced on the metal atom and increased on the ligand. In addition to their sensitivity to the nature of the ligands, to cis- versus trans-coordination and to the number of ligands (Pt(II) versus (IV), in particular), platinum NMR chemical shifts are also known to be sensitive to solvent effects[9,16−18] and temperature.[9] Likewise, Pt − ligand NMR *J*-coupling has been demonstrated to be very sensitive to the presence of solvent.[18,19] For instance, we have shown recently that in cisplatin and derivatives thereof, roughly half of the magnitude of the *J* (Pt−N) coupling constants results from weak coordination of solvent molecules (water, in this case) to the metal center.[18] For anionic complexes, computations have further indicated a strong sensitivity of Pt chemical shifts to metal−ligand bond distances.[20,21]

Herein, we continue a series of theoretical studies of NMR parameters for Pt complexes of actual or potential antitumor activity[17,18] and focus on complexes with azide ligands because of the aforementioned potential as photoactivatable agents.

Received: April 27, 2012
Published: July 14, 2012

   dx.doi.org/10.1021/ja3040762 | *J. Am. Chem. Soc.* 2012, 134, 13374−13385

Along with ^{195}Pt chemical shifts and Pt–ligand *J*-coupling constants, Farrer et al.[22] recently reported experimental ^{14}N and ^{15}N NMR spectroscopic data for a number of platinum azido complexes shown in Figure 1. Nitrogen has two NMR-active isotopes, ^{14}N and ^{15}N. Even though ^{14}N has a high natural abundance (99.63%), it is the ^{15}N nucleus that has been more commonly utilized in NMR experiments. This is mainly due to the nonvanishing electric quadrupole moment of the spin-1 isotope ^{14}N, which implies that for less symmetric environments, the quadrupolar interaction with the local electric field gradient (EFG) results in significant anisotropic broadening of spectral lines. The low resonance frequency of 43.3 MHz (compared to 600 MHz for ^{1}H) at 14.1T also makes the detection of ^{14}N signals difficult. The application of antiringing pulse sequences allowed Farrer et al. to improve substantially the time needed to acquire high-quality spectra. For the spin-1/2 isotope, ^{15}N which has a natural abundance of only 0.37%, the sensitivity of detection has been enhanced by ^{15}N isotope enrichment and the use of proton-detected inverse methods where applicable.[23] As expected, the azido ligand proved to be challenging due to the nonzero quadrupolar moment of the ^{14}N nuclei. In addition, there is a lack of protons around N_3 that otherwise may help to enhance the ^{15}N signal by transferring nuclear spin polarization from ^{1}H to ^{15}N.

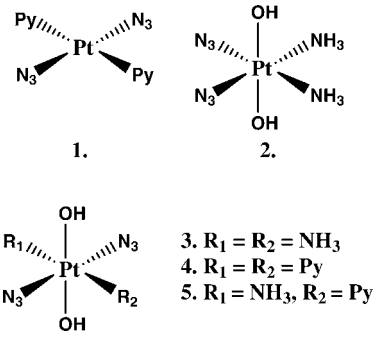

Figure 1. Pt-azido complexes studied in this work: **1** = *t*-[$Pt(N_3)_2(Py)_2$]; **2** = *ctc*-[$Pt(N_3)_2(OH)_2(NH_3)_2$]; **3** = *ttt*-[$Pt(N_3)_2(OH)_2(NH_3)$]; **4** = *ttt*-[$Pt(N_3)_2(OH)_2(Py)_2$]; and **5** = *ttt*-[$Pt(N_3)_2(OH)_2(NH_3)(Py)$], where the notation means *t* = trans, *c* = cis, *ctc* = *cis,trans,cis*, and *ttt* = *trans,trans,trans*. Other Pt complexes included in the discussion in Section 3 are: **6** = *t*-[$PtCl_2(Py)_2$]; **7** = *c*-[$Pt(NH_3)_2(N_3)_2$]; **8** = *c*-[$Pt(NH_3)_2(OH)_2$]; and **9** = *c*-[$Pt(NH_3)_2(Cl)_2$].

The experimental data exhibit very interesting trends that warrant investigation by first-principles theory. The nitrogen directly coordinated to Pt, N_α, affords substantially broadened ^{14}N signals as quantified, for example, by the peak width at half-height of ≈2124 Hz for N_α in the complex **4** compared to only 142 Hz for N_β the central nucleus of N_3.[22] Furthermore, there is a pronounced shielding of N_α in the azido ligands compared to the terminal nitrogen, N_γ, despite N_α donating electron density to Pt. In free azide the two nitrogens are of course equivalent. Finally, the N_β azide nuclei afford particularly high chemical shifts (low magnetic shielding).

We aim to unravel, with the help of localized molecular orbital (LMO) analyses of the calculated electric field gradients, why the ^{14}N NMR signal for N_β (the middle N) in azide ligands is so sharp compared to N_α and N_γ which are extremely broadened. A similar LMO analysis technique has been used successfully recently in a study of ^{14}N quadrupolar interactions in solids of biologically relevant molecules.[24] Another aim is to illustrate why the coordination of azide to platinum increases the shielding of N_α relative to N_γ and why the N_β nuclear shielding constants are particularly small in magnitude. In a simplistic model where the shielding is related to the effective electron number, the high N_α shielding is unintuitive because of the dative $N_\alpha \rightarrow$ Pt bond. However, there may be competing trends related to how effectively or not the magnetic field can induce paramagnetic current densities around N_α in the free ligand and in the complex, and because of the vicinity to Pt, there is the question of how important are relativistic effects from the nearby heavy atom. Last but not least, we report calculations of Pt chemical shifts and Pt–N spin–spin coupling constants for the set of azide complexes. There is a growing number of theoretical studies demonstrating that Pt chemical shifts and Pt–ligand *J*-coupling (which require a relativistic quantum chemical approach and a high-quality computational model) can be difficult to predict accurately from first principles theory.[21,25−31] In previous work we put forward computational models for Pt complexes in aqueous solution that allow for efficient Pt NMR parameter calculations of acceptable quality.[16−18] Herein, we further test and validate these computational protocols.

This article is organized as follows: In Section 2 the computational setup is described along with technical details. Computed NMR data and the EFGs are then analyzed and compared with experiment (Section 3). This work concludes with a brief summary of key findings and an outlook (Section 4).

2. COMPUTATIONAL DETAILS

Density functional theory (DFT) calculations of ^{195}Pt and ^{15}N NMR shielding tensors, *J*-coupling constants, and EFGs were performed with the Amsterdam Density Functional (ADF)[32] package. Experimental geometries from single-crystal X-ray diffraction (XRD) data[2] were used as starting structures for DFT optimizations. Optimized structures were employed in the NMR and EFG computations. Relativistic effects were considered by means of the all-electron relativistic zeroth-order regular approximation (ZORA)[33] in its spin–orbit (SO) two-component form for shielding and *J*-coupling and in the scalar relativistic approximation in which SO coupling is neglected for EFGs and geometry optimizations. The NMR calculations were based on the ZORA methods reported in refs 34–38. Chemical shifts are reported here with respect to the references $[PtCl_6]^{2-}$ (aq) and $^{14/15}NH_3$ for ^{195}Pt and $^{14/15}$N, respectively, using the chemical shift definition[39] $\delta = (\sigma^{ref} - \sigma)/(1 - \sigma^{ref})$ in its approximate form $\delta \approx (\sigma^{ref} - \sigma)$. Shielding constants and chemical shifts are given in ppm. The LMO analysis of EFGs was performed with the methods described in ref 40. The NMR shielding analysis utilized an analysis method based on spin-free LMOs as described in refs 41 and 42. The LMOs were generated with the natural bond orbital (NBO) algorithms using a locally modified version of the NBO 5.0 program.[43] Specifically, the analyses utilized the 'natural localized molecular orbitals' produced by the NBO algorithms.[44]

The revised Perdew–Burke–Ernzerhof (revPBE) functional[45] was used for all calculations. For benchmarks with Pt complexes, see refs 16–18, 21, and 46. ZORA-optimized triple-ζ doubly polarized (TZ2P) Slater-type basis sets for the ligand atoms and the quadruple-ζ quadruply polarized (QZ4P) ZORA basis for Pt (both from the ADF basis set library)[32] were employed. The conductor-like screening model (COSMO)[47] was applied to treat solvent effects (aqueous solution). To construct the solvent surface a solvent radius of 1.4 Å and a dielectric constant of 78.8 was used in the COSMO setup. The atomic radii in COSMO may influence computed result to some degree. The following radii for the atomic radii were utilized (in Å): Pt = 2.1, Cl = 1.8, O = 1.3, N = 1.4, and H = 1.2.[18,48,49] Previous

dx.doi.org/10.1021/ja3040762 | J. Am. Chem. Soc. 2012, 134, 13374–13385

Table 1. Optimized Structural Parameters of the Complexes of Figure 1 and Free Azide[a]

	N_α–N_β–N_γ	Pt–N_α–N_β	N_α–N_β	N_β–N_γ	Pt–N_α	Pt–NH_3	Pt–NPy	Pt–OH
1	174.6	120.7	1.218	1.170	2.068		2.049	
	(174.5)	(125.4)	(1.188)		(2.036)		(2.031)	
2	174.2	118.1	1.223	1.162	2.066	2.091		2.048
3	174.5	118.3	1.222	1.163	2.086	2.066		2.039
4	175.0	118.0	1.221	1.164	2.093		2.076	2.037
	(174.8)	(119.1)	(1.216)	(1.143)	(2.045)		(2.047)	(2.009)
5	174.7	118.1	1.222	1.164	2.090	2.067	2.069	2.038
N_3^-	180		1.201	1.201				

[a]Selected bond distances (Å) and bond angles (°). XRD distances and angles in parentheses. Structures downloaded from Cambridge Crystallographic Data Centre using the access code CCDC 777420, ref 2. Geometries optimized with scalar-ZORA/COSMO/revPBE.

Table 2. Calculated ^{15}N NMR Azide Ligand Shielding Constants (σ) and Chemical Shifts (δ), in ppm, for Various Platinum Azido Complexes and Azide[a]

	$^{15}N_\alpha$			$^{15}N_\beta$			$^{15}N_\gamma$		
complex	σ	δ	exptl	σ	δ	exptl	σ	δ	exptl
t-$[Pt(N_3)_2(Py)_2]$	165.5	15.9	5.8	−13.0	194.4	210.5	82.5	98.9	115.3
ctc-$[Pt(N_3)_2(OH)_2(NH_3)]$	150.6	30.7	21.5	−11.6	193.0	207.8	49.6	131.8	147.5
ttt-$[Pt(N_3)_2(OH)_2(NH_3)]$	142.9	38.5	24.8	−13.1	194.4	207.8	37.4	144.0	146.2
ttt-$[Pt(N_3)_2(OH)_2(Py)_2]$	130.9	50.5	42.1	−12.8	194.1	209.0	30.6	150.7	150.8
ttt-$[Pt(N_3)_2(OH)_2(NH_3)(Py)]$	136.9	44.5	28.8	−12.8	194.2	208.8	33.8	147.6	144.5
azide	146.6	40.6		−12.0	199.1		146.6	40.6	
azide (5°)	145.7	41.4		−12.2	199.3		145.7	41.5	

[a]The azide (5°) structure has been bent by 5° with bond lengths maintained the same as those of linear azide. Experimental chemical shifts obtained from ref 22 and converted from the reference of 1.5 M NH_4Cl in 1 M HCl to liquid ammonia by subtraction of 20.1 ppm (based on the chemical shifts of NH_4Cl and ammonia with respect to CH_3NO_2 provided in ref 22). Liquid ammonia has a chemical shift of 380.23 ppm with respect to the primary reference, neat nitromethane. All experimental values are based on ^{14}N NMR with an exception of *ttt*-$[Pt(N_3)_2(OH)_2(Py)_2]$ and *ttt*-$[Pt(N_3)_2(OH)_2(NH_3)(Py)]$. Isotropic chemical shifts were calculated using a theoretical reference value of σ^{ref} = 181.4 ppm for liquid NH_3 obtained from fitting $\sigma^{calc} = -\delta^{exptl} + \sigma^{ref}$. For comparison, a calculation for an ammonia molecule gave σ (calcd) = 201.6 ppm.

Table 3. Calculated ^{195}Pt and ^{15}N NMR Shielding (σ) and Chemical Shifts (δ), in ppm, for Various Platinum Azido Complexes[a]

	^{195}Pt			^{15}NPy			$^{15}NH_3$		
complex	σ	δ	exptl	σ	δ	exptl	σ	δ	exptl
t-$[Pt(N_3)_2(Py)_2]$	3699.8	−1922.0	−2122	17.9	163.5	161.6			
ctc-$[Pt(N_3)_2(OH)_2(NH_3)]$	1370.6	407.2	–				242.4	−61.1	−58.4
ttt-$[Pt(N_3)_2(OH)_2(NH_3)]$	1432.1	345.8	858				237.2	−55.8	−60.8
ttt-$[Pt(N_3)_2(OH)_2(Py)_2]$	1471.4	306.4	942	14.8	166.6	148.8			
ttt-$[Pt(N_3)_2(OH)_2(NH_3)(Py)]$	1431.3	346.5	913	23.5	157.8	154.8	230.2	−48.9	−66.8
t-$[PtCl_2(Py)_2]$	3501.8	−1724.0	−1958	17.0	164.4	159.1			

[a]Experimental chemical shifts for ^{195}Pt were obtained from ref 22 referenced to $PtCl_6^{2-}$. The computed isotropic nuclear shielding for this reference is σ (^{195}Pt) = 1777.8 ppm which was used to obtain the calculated δ (^{195}Pt). Nitrogen chemical shifts were obtained as described in the footnotes of Table 2.

calculations of NMR parameters of cisplatin and derivatives thereof utilizing these COSMO parameters yielded reasonable agreement with experimental data and with computations where the solvent was treated explicitly, quantum mechanically, in molecular dynamics simulations.[17,18]

3. RESULTS AND DISCUSSION

3.1. Geometries. Selected optimized structural parameters for the complexes of Figure 1 are collected in Table 1. XRD data were extracted from structures reported by Farrer et al.[2,22] The agreement of optimized with experimental structural parameters is reasonable. Bond angle variations typically have shallower potentials than bond distances and are easily influenced by crystal packing, which explains differences of the Pt–N_α–N_β angles between the XRD structures and the optimized geometries. Compared to free azide, the N_β–N_γ distance shortens, while the N_α–N_β distance expands slightly upon formation of the $N_\alpha \rightarrow$ Pt dative bond. The calculated bond orders discussed in Section 3.3 are in line with the structural trend. The azide ligand in the Pt complexes is bent by about 5°. The optimized bond length of the free N_3^- molecule appears reasonable when compared to gas-phase experimental distances of 1.188 Å for N_3^- and 1.181 Å for the N_3 radical.[50,51] We note that the class of generalized gradient approximation (GGA) functionals, of which revPBE is a member, has a tendency to overestimate slightly bond distances in covalently bound systems.

3.2. ^{15}N and ^{195}Pt NMR Chemical Shifts and *J*-Coupling Constants. Collected in Tables 2 and 3 are ^{15}N and ^{195}Pt nuclear shielding constants (σ) and chemical shifts (δ) for the various platinum complexes. The SO ZORA calculations based on COSMO with the QZ4P basis for Pt were found to agree better with experiment than calculations with

dx.doi.org/10.1021/ja3040762 | J. Am. Chem. Soc. 2012, 134, 13374–13385

less flexible basis sets or without the solvent model. Additional calculated data can be found in Table S1 of the Supporting Information (SI). The nuclear shielding constants are provided in order to enable conversion to an alternate reference. All experimental nitrogen shifts are with reference to liquid ammonia. Computations for this reference would require an elaborate computational model because dynamic hydrogen bonding is certain to impact the N shielding. Since there are several data points for azide, ammonia, and pyridine ligands available, a theoretical value for the reference was instead determined from a linear fit of σ(calcd) versus $-\delta$(exptl) (see footnotes of Table 2). The computed ^{15}N NMR chemical shifts exhibit reasonable agreement with experiment. A graphical comparison of calculations versus experiment for the nitrogen chemical shifts for azide, pyridine, and amine ligands is shown in Figure 2. The clustering of data clearly reflects the chemical shifts from the various types of nitrogen centers in the complexes. Of particular interest is the differences in the chemical shifts for different nitrogen atoms in the azide ligands. N_α has a significantly lower chemical shift (larger shielding) than N_β and N_γ, with the central nitrogen (N_β) affording the highest chemical shift/lowest nuclear shielding. The calculations correctly reproduce the trends seen experimentally, in terms of both shift ordering and shift differences.

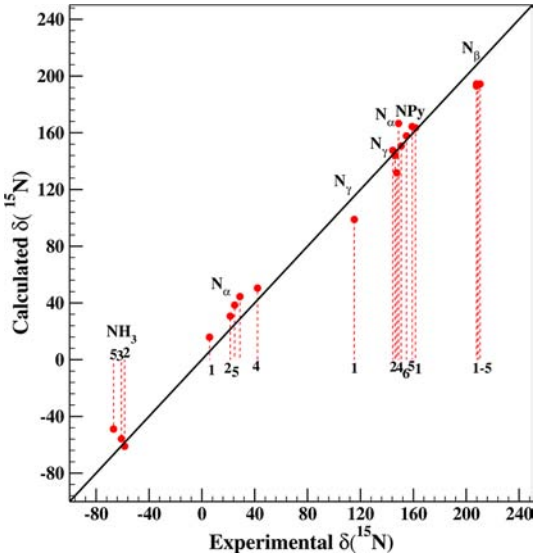

Figure 2. Correlation between experimental and calculated ^{15}N NMR chemical shifts for the complexes **1** = *t*-[Pt(N$_3$)$_2$(Py)$_2$]; **2** = *ctc*-[Pt(N$_3$)$_2$(OH)$_2$(NH$_3$)]; **3** = *ttt*-[Pt(N$_3$)$_2$(OH)$_2$(NH$_3$)]; **4**= *ttt*-[Pt(N$_3$)$_2$(OH)$_2$(Py)$_2$]; **5** = *ttt*-[Pt(N$_3$)$_2$(OH)$_2$(NH$_3$)(Py)]; and **6** = *t*-[PtCl$_2$(Py)$_2$] (see Figure 1).

In a free unperturbed azide molecule, the two terminal nitrogens, N_α and N_γ, would be equivalent. Upon coordination of azide to platinum, N_α becomes more shielded than N_γ (less positive chemical shift). Naively, donation of electron density from N_α to Pt may be expected to lead to a deshielding of N_α if the effective number of electrons around the nucleus is the main influence (nuclei in electron-rich atoms are more shielded than nuclei in light atoms). However, the change in the electron distribution causes other important effects that may lead to a more or less effective induction of paramagnetic current densities around N_α, which may, in the end, run counter-intuitive to the simple electron number argument. As an example, if the gaps between occupied and unoccupied orbitals relevant to the paramagnetic shielding term increase, the resulting total shielding may decrease.[52] However, numerical studies have shown that the orbital gaps alone are not always indicative of the shielding trends,[53] and detailed numerical analyses are usually called for. In a later section the N_α trend is analyzed in detail for one of the complexes, along with the particularly high chemical shifts observed for N_β.

Given the known sensitivity of Pt chemical shifts discussed in the Introduction, the agreement of the calculations with experiment can be considered acceptable when keeping in mind the very large chemical shift range of Pt (for results see Table 3 and Table S1 of the SI). Improved results, with error bars of a few hundred ppm, can be expected from molecular dynamics based averaging of the shifts with explicit solvation at the quantum mechanical level.[16−18] Systematic improvements of calculated Pt chemical shifts toward error bars that are reliably below 100 ppm would likely require a high-level correlated wave function approach within an all-electron relativistic framework, which is presently out of reach. By far the most obvious trend (and largest in magnitude) is the shift difference between Pt(II) and Pt(IV). We have analyzed and explained this difference in a previous paper.[42] In a nutshell, the magnetic field can induce strong deshielding paramagnetic current densities in the 5d shell of six-coordinate Pt(IV) complexes for each direction of the magnetic field. In four-coordinate Pt(II) complexes, the negative paramagnetic shielding tensor components are much smaller for field directions parallel to the complex plane because of a lack of unoccupied metal−ligand σ^* orbitals perpendicular to the complex plane. See ref 42 for an 'orbital rotation' model for d orbitals rationalizing the difference between Pt(II) and Pt(IV). The net result is a stronger magnetic shielding of Pt(II) compared to Pt(IV) and a concomitant negative chemical shift

Table 4. Calculated J^{195}_{Pt-15N} for Pt−Azido Complexes Compared to Available Experimental Data (in parentheses)[a]

	NPy	NH$_3$	N$_\alpha$	N$_\gamma$	N$_\beta$
complex	$^1J_{Pt-N}$	$^1J_{Pt-N}$	$^1J_{Pt-N}$	$^2J_{Pt-N}$	$^3J_{Pt-N}$
t-[Pt(N$_3$)$_2$(Py)$_2$]	−435.6		−185.9	−1.4	−37.0
ctc-[Pt(N$_3$)$_2$(OH)$_2$(NH$_3$)]		−259.0(258)[b]	−216.4	−0.3	−22.5
ttt-[Pt(N$_3$)$_2$(OH)$_2$(NH$_3$)]		−269.1(261)[a]	−158.3	5.3	−24.7
ttt-[Pt(N$_3$)$_2$(OH)$_2$(Py)$_2$]	−381.9(370)		−159.8(223)	5.7	−26.9(20)
ttt-[Pt(N$_3$)$_2$(OH)$_2$(NH$_3$)(Py)]	−355.7	−287.5(291)	−156.8(212)	5.9	−25.6[c]
t-[PtCl$_2$(Py)$_2$]	−389.7(400)				

[a]All coupling constants are in Hz. Experimental data from ref 22. Signs of the experimental *J*-couplings were not determined. *J*-couplings values computed with SO ZORA/COSMO/revPBE. [b]The experimental value initially obtained for ^{14}N was converted to ^{15}N as explained in the text. [c]Ref 54.

of Pt(II) with respect to a Pt(IV) reference which may exceed 2000 ppm in magnitude. The data in Table 3 clearly reflect this difference. We note in passing that it is particularly challenging to calculate reliable chemical shifts of solvated Pt complexes with different Pt oxidation states relative to each other.[21]

A final assessment of the computations considers the *J*-coupling constants between Pt and ligand nitrogen atoms. *J*-coupling can provide important insight into the extent of covalent interaction between a metal center and the coordinated ligands, and it may yield clues about the geometry of a complex (e.g., cis vs trans coordination). A compilation of J_{PtN} can be found in Table 4, and additional data comparing various levels of theory are compiled in Tables S2 and S3 of the SI. Figure 3 graphically displays the correlation between

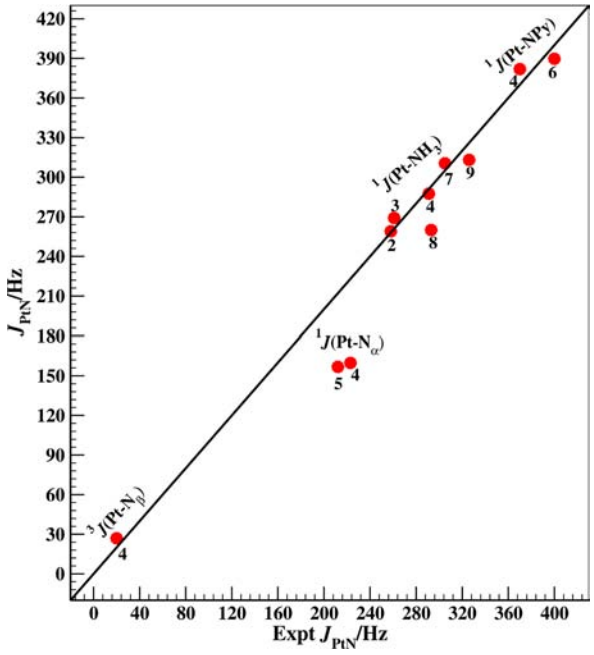

Figure 3. Calculated versus experimental $J_{^{195}Pt-^{15}N}$ for complexes numbered as in Figure 1 and its caption. Computed values for complexes **8** and **9** were taken from ref 18.

calculated and experimental data. For comparison, additional *J*-coupling data from ref 18 were included. Calculated *J*-couplings for ^{14}N were scaled using $\gamma_{^{15}N}/\gamma_{^{14}N} = -1.403$, the gyromagnetic ratios of the two nitrogen isotopes, to convert to ^{15}N. As expected, the $^1J_{PtN}$ is substantially larger than the $^2J_{PtN}$ and $^3J_{PtN}$ couplings. The three-bond coupling of the azide N_γ with Pt is sizable, with reasonable agreement of the calculated value for complex **5** and experiment. The calculated Pt–N_α couplings would likely improve in calculations with explicit solvent and molecular dynamics based averaging.

An influence of trans ligands can be seen by considering the azide $^1J_{PtN_\alpha}$ where we note a change of about 58 Hz between the *ctc* (**2**) and *ttt* (**3**) isomers of $Pt(N_3)_2(OH)_2(NH_3)$. The coupling constant change correlates with a change of the bond distances Pt–N_α by about 0.02 Å between the two complexes. One might be tempted to conclude that the covalent bond character between the azide ligands and platinum is the weakest in comparison to Pt–NPy or Pt–NH_3, since the ^1J (Pt–N_α) are smallest in magnitude while the Pt–N bond distances are comparable. The calculated N–Pt bond orders for all ligands are comparable, however, around 0.4. The formal sp hybridization of the azide N_α would normally be expected to give large *J*-coupling constants. We show in Section 3.3 that the N_α–Pt bond has in fact a very small N_α s-character which means that the spin polarization transfer between the nuclei is facilitated by a more indirect mechanism additionally involving an s-rich N_α lone pair (LP), which is the reason for these small *J*-couplings. We note in passing that, for example, the spin mechanism (Fermi-contact and spin-dipole) constitutes 83% of the total *J* (Pt–N_α) of complex **3**, while the paramagnetic nuclear spin–electron orbital current mechanism (PSO) make up for the remaining 17%. As usual, the diamagnetic orbital current mechanism is negligible. The $^1J_{Pt-NPy}$ are the largest among those listed in Table 4, and significantly larger in magnitude than the $^1J_{Pt-NH_3}$ coupling constants. The relative magnitudes are easily rationalized by the formal sp^2 hybridization of the pyridine nitrogen compares to the formal sp^3 hybridization for the amine ligand, since a larger s-character gives larger Fermi-contact terms in *J* if all other factors are equal.[55]

3.3. Bonding in Free Azide and in the Azido Ligands.

The chemical shifts and EFGs in the azido ligands are most conveniently discussed in relation to a symmetric free azide molecule. Shown in Figure 4 is the Lewis structure of free azide,

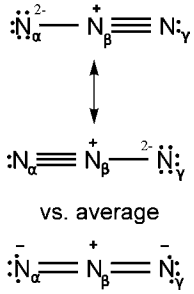

Figure 4. Top: Resonance structures of free azide derived from NBO calculations. Bottom: The 'average' yields a Lewis structure of azide as depicted in textbooks.

N_3^-, as derived from NBO calculations alongside a Lewis structure as it is commonly shown in chemistry textbooks. The LMOs representing the Lewis electron pairs, obtained from the DFT calculation, are shown in Figure 5. For a delocalized

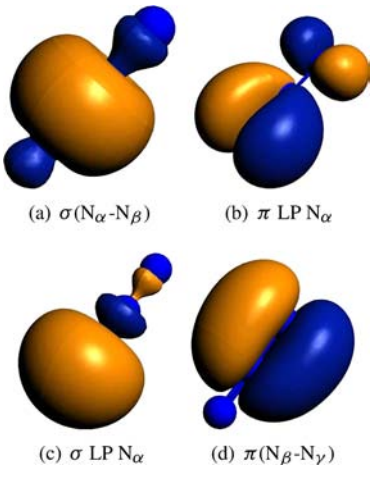

Figure 5. Selected LMOs of free azide (isosurfaces, ± 0.03 au). One of two equivalent π orbitals is shown for π (N_β–N_γ) and the N_α π LPs.

dx.doi.org/10.1021/ja3040762 | J. Am. Chem. Soc. 2012, 134, 13374–13385

system with multicenter bonding, the NBO algorithms typically produce one of several possible resonance structures. In our case, the calculations yielded a single-bond triple-bond Lewis structure, as shown at the top left of Figure 4. The electron density has the full symmetry of free azide, but the breakdown in terms of σ and π lone pair (LP) and bonding contributions is not necessarily symmetric. An equivalent Lewis structure would afford the triple bond between N_α and N_β instead, and the average is symmetric. The textbook Lewis structure with two double bonds in a sense corresponds to the average of these two resonance forms. A textbook Lewis structure with distinguishable localized π bonds and lone pairs would not be cylindrically symmetric. The two resonance structures have electron densities that are symmetric with respect to rotations about the molecule axis. Within the NBO framework, the fact that the calculation gives one of the Lewis resonance structures reflects the presence of two 3-center-4-electron (3c4e) π bonds in this system. Note the strong delocalization of the N_α π 'LP' orbitals in Figure 5; only 67% of their density is associated with hybrid orbitals centered on N_α. Indeed, an additional NBO calculation with the '3CHB' keyword assigned the presence of two symmetric 3c4e bonds in azide. For the LMO analysis, it is important to keep in mind that the two terminal nitrogens in free azide have identical field gradients NMR shielding constants when all LMO contributions are added.

The azide electronic structure changes significantly upon formation of the dative ligand−Pt bonds. Figure 6 displays

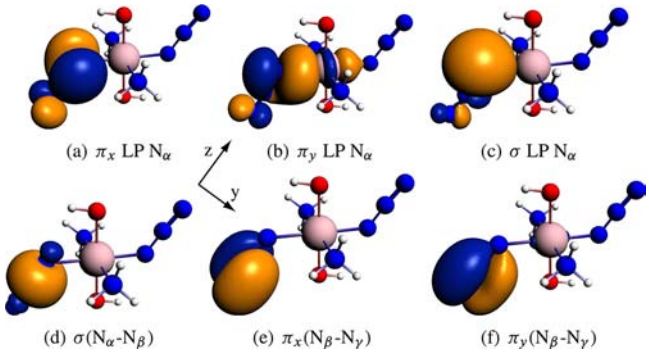

Figure 6. *ttt*-$[Pt(N_3)_2(OH)_2(NH_3)]$ (**3**): Selected LMOs (isosurfaces, ± 0.03 au). The dative N_α−Pt bond ($N_\alpha \rightarrow$ Pt) is formed by the π_y LP N_α LMO. Also shown is a local coordinate frame for azide used to label the azide-centered LMOs. The *x* axis points toward the reader.

LMO isosurfaces for complex **3** which was taken as a representative for the azido complexes set of Figure 1. Additional data and figures for the other complexes can be found in Tables S4 and S5 and Figures S1−S4 of the SI. In the Pt complex, the NBO-derived Lewis structure for the azido ligands also affords a single-bond triple-bond pattern with the single bond between N_α and N_β, but obviously N_α and N_γ are now inequivalent. Table 5 gives an account of the atomic hybrid orbital contributions to selected LMOs in free azide and in complex **3**. The LMO isosurface plots for complex **3** show that the LMO labeled as the π_y 'LP' of N_α is in fact the N_α−Pt σ bonding orbital. The covalent character is significant, with a Wiberg bond index (WBI), a measure for the bond order, of 0.42 (31% of the orbital's density is centered on Pt). The π_x orbital remains of local π symmetry with respect to the N_α−Pt axis. The ligand−metal bonding involving the (distorted) N_α π LP is facilitated by the non-linear N_β−N_α−Pt arrangement. The

Table 5. Compositions of Selected LMOs in the N_3 Moiety in Terms of Atomic s/p/d/f Contributions for Free Azide and Complex 3 (*ttt*-$[Pt(N_3)_2(OH)_2(NH_3)]$)[a]

	azide, N_3^-		complex **3**	
WBI(N_α−N_β)	1.93		1.64	
WBI(N_β−N_γ)	1.93		2.20	
WBI(N_α−Pt)			0.42	
σ (N_α −N_β)				
N_α	44	s[29]p[70]	44	s[28]p[72]
N_β	56	s[49]p[51]	56	s[49]p[51]
σ LP N_α				
N_α	98	s[71]p[29]	93	s[68]p[32]
π_x LP N_α				
N_α	67	s[0]p[100]d[0]	73	s[0]p[100]d[0]
N_β	17	s[0]p[99]d[1]	13	s[0]p[99]d[1]
N_γ	16	s[0]p[100]d[0]	14	s[0]p[100]d[0]
π_y LP N_α				
N_α	67	s[0]p[100]d[0]	57	s[6]p[94]d[0]
N_β	17	s[0]p[99]d[1]	5	s[1]p[97]d[2]
N_γ	16	s[0]p[100]d[0]	6	s[0]p[100]d[0]
Pt			31	s[13]p[0]d[87]
π_x (N_β−N_γ)				
N_β	47	s[0]p[100]d[0]	50	s[0]p[100]d[0]
N_γ	52	s[0]p[100]d[0]	49	s[0]p[100]d[0]
π_y (N_β−N_γ)				
N_β	47	s[0]p[100]d[0]	56	s[1]p[99]d[0]
N_γ	52	s[0]p[100]d[0]	42	s[1]p[99]d[0]
Pt			1	s[4]p[1]d[95]

[a]All numerical values in %. WBI = calculated Wiberg bond index. N_α 44 s[29]p[70] means that 44% of the orbital is associated with hybrids centered on N_α, with 29% s and 70% p character overall.

strongly delocalized character of π_y is still apparent in the figure, but it is weaker than for free azide. This is evident from the LMO compositions listed in Table 5 and in Tables S4 and S5 of the SI for the other complexes. The relatively small Pt−N_α *J*-couplings must be a consequence of the Pt−N_α bond being facilitated by an orbital with only 6% nitrogen s character. The fact that the spin mechanism dominates the coupling renders it likely that spin polarization being transferred between the nuclei involves a coupling of the π_y and σ LP LMOs.

Along with the N_α−Pt bond formation goes a decrease in the N_α−N_β bond order from 1.9 in free azide to 1.6 in the complex and an increase in the N_β−N_γ bond order from 1.9 to 2.2. Similar trends are found for the other azido complexes (see Tables S4 and S5 of the SI), i.e., the azide ligand retains some of the π delocalization of free azide, but overall the electronic structure becomes more localized, giving more weight to the Lewis structure at the top of Figure 4. Further, there is a rehybridization taking place at N_α upon complexation in two ways: First, the nonlinear environment of N_α in the complex allows some mixing of nitrogen 2s with the formerly pure $2p_\pi$ orbitals. The s content of the π_y LP/bond remains small, however. Likewise, the s-rich N_α σ LP of free azide remains s-rich. A second effect is clearly seen in Figure 6 and Figure S3 of the SI: There is p_y−p_z mixing (*z* referring to the N_3 axis) in the π_y LP as well as in the σ LP on N_α, allowing for a local rotation of the N_α hybrids to facilitate the azide−Pt bonding. It is shown in Sections 3.4 and 3.5 that this rehybridization creates strong changes in the LMO contributions to the NMR shielding at N_α but leaves the sum from the N_α LPs almost unchanged. However, there is a strong effect on the N_α field gradient.

dx.doi.org/10.1021/ja3040762 | J. Am. Chem. Soc. 2012, 134, 13374−13385

Table 6. ^{14}N EFG Tensor Parameters V_{33} and η for N_3^-, Pyridine, and the Platinum Azido Complexes of Figure 1

complex	NPy	NH_3	N_α	N_β	N_γ
V_{33}, au					
t-[$Pt(N_3)_2(Py)_2$]	−0.389		0.683	−0.132	−0.364
ctc-[$Pt(N_3)_2(OH)_2(NH_3)$]		−0.346	0.734	−0.125	0.446
ttt-[$Pt(N_3)_2(OH)_2(NH_3)$]	–	−0.246	0.708	−0.121	0.380
ttt-[$Pt(N_3)_2(OH)_2(Py)_2$]	−0.256	–	0.693	−0.121	−0.402
ttt-[$Pt(N_3)_2(OH)_2(NH_3)(Py)$]	−0.245	−0.256	0.700	−0.121	0.385
t-[$PtCl_2(Py)_2$]	−0.362	–	–	–	–
azide			0.442	−0.148	0.442
pyridine	−1.040				
η					
t-[$Pt(N_3)_2(Py)_2$]	0.079	–	0.560	0.935	0.487
ctc-[$Pt(N_3)_2(OH)_2(NH_3)$]		0.170	0.839	0.788	0.799
ttt-[$Pt(N_3)_2(OH)_2(NH_3)$]	–	0.103	0.758	0.527	0.890
ttt-[$Pt(N_3)_2(OH)_2(Py)_2$]	0.122	–	0.796	0.701	0.956
ttt-[$Pt(N_3)_2(OH)_2(NH_3)(Py)$]	0.143	0.107	0.774	0.583	0.964
t-[$PtCl_2(Py)_2$]	0.144	–	–	–	–
azide			0.000	0.000	0.000
pyridine	0.386				

3.4. EFG Analysis. As pointed out in the Introduction, the NMR signal of the azido $^{14}N_\alpha$ is broader than those for $^{14}N_\beta$ and $^{14}N_\gamma$. This can be attributed to a strong inhomogeneity of the electric field, quantified by the EFG, at the N_α nucleus in the coordinated platinum complexes. For N_β, the signal broadening is particularly small, hence one expects a particularly small EFG at the central nitrogen in the azido ligand.

The data reported in this section are for V_{33}, the largest-magnitude principal component of the field gradient tensor, and the asymmetry parameter $\eta = (V_{11} - V_{22})/V_{33}$. We refer to V_{33} and the other principal components of the tensor V as the electric field gradient, as it is commonly done,[40] keeping in mind the negative sign with respect to the field gradient proper. The EFGs are reported in atomic units (au). The conversion to the nuclear quadrupole coupling constant (NQCC, or C_Q) is $C_Q = (e/h)\ QV_{33}$, where Q is the nuclear quadrupole moment.[56] To convert 1 au of field gradient to C_Q in MHz, the conversion is 0.2350·Q MHz/mbarn with Q in units of mbarn (10^{-31} m^2). For ^{14}N, the conversion factor works out to be 4.803 MHz.

For free azide and the azido complexes investigated herein, the calculated V_{33} for N_α, N_β, and N_γ and the corresponding asymmetry parameters are listed in Table 6. In all cases the N_β field gradient is substantially smaller in magnitude than those of the terminal azido nitrogens. Moreover, binding of N_α to platinum is seen to increase its EFG significantly compared to free azide, while at the same time the EFG of N_γ in the complexes becomes smaller in magnitude (but it remains much larger than the EFG of N_β). Therefore, the trends in the calculated EFGs correctly represent the experimental findings about the ^{14}N NMR signal broadening. Along with the increase of the EFG at N_α upon complexation, η parameters indicate substantial deviation from axial symmetry. For N_α this asymmetry is related to the roughly 120° Pt−N_α−N_β angles (Table 1) and for N_β and N_γ to the approximately 5° bending of the azide moiety as well as electrostatic effects from nearby atoms in the remainder of the complex. For two of the complexes (**1** and **4**), V_{33} at N_γ has the opposite sign than in free azide. Representative visualizations of EFG tensors are shown in Figures S1, S2 and S3 of the SI. The apparent sign change simply reflects the fact that a principal component along a different direction becomes the largest in magnitude; otherwise the N_γ tensors have comparable characteristics and orientations to that of complex **3** shown in Figure 7 (see below for discussion).

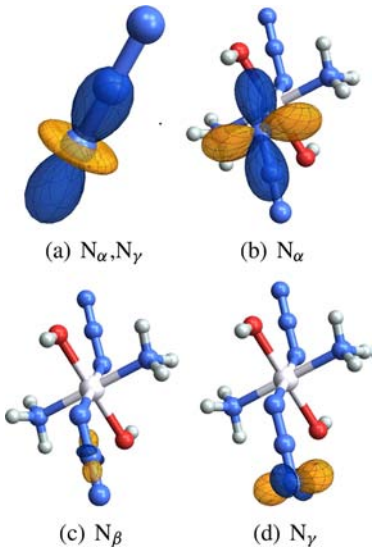

Figure 7. Graphical representations of the EFG tensors of azide (a) and for the platinum azido complex **3** (b−d). The functions graphed here in form of polar plots are $f = s\sum_{uv} u V_{uv} v$, where V_{uv} are the Cartesian EFG tensor components and $u, v \in \{x, y, z\}$, as explained in ref 40. The scaling factors, s, for (a−d) are 350, 300, 700, and 350 au/pm respectively. Blue color (dark shading) indicates a positive EFG, while yellow (light shading) indicates a negative EFG. V_{33} = +0.442, +0.708, −0.121, and +0.380 au for (a−d), respectively.

EFG data for selected amine and pyridine (NPy) nitrogens are also listed in Table 6. The V_{33} for these ligands are negative. For amine they are uniformly smaller in magnitude than those for the azide N_α. For isolated pyridine, V_{33} is very large in magnitude. The case of ammonia (and other systems) has been analyzed previously[40] with an atomic hybrid model for the EFG somewhat akin to the old Townes−Dailey model.[57] The

dx.doi.org/10.1021/ja3040762 | J. Am. Chem. Soc. 2012, 134, 13374−13385

nitrogen V_{33} for free ammonia is about −0.8 au, with the principal axis associated with V_{33} pointing along the direction of the LP sp^3 hybrid. The negative sign is consistent with excess electron density around nitrogen from the nitrogen LP relative to the bonding hybrids for which electron density is shared with the hydrogens.[40] For pyridine, the situation is qualitatively similar. An sp^2 hybrid model shows that strong delocalization of electron density associated with the nitrogen p_π orbital leads to a particularly large negative field gradient component in the direction of the sp^2 LP orbital.[40] The formation of dative bonds from the ammonia as well as pyridine nitrogens to the Pt centers in the various complexes significantly reduces the magnitude of the EFG. Based on a consideration of the EFG in terms of atomic hybrid orbitals, this change is easy to explain: Sharing of electron density from the nitrogen LP with the metal center reduces the electron density and the magnitude of the negative EFG contribution from the donor hybrid at the ligand nitrogen.

For free azide, the calculated V_{33} are equal and positive for N_α and N_γ. For the central nitrogen, N_β, the EFG is of much smaller magnitude and negative. The asymmetry parameters are zero, as expected, due to the cylindrical symmetry of N_3^-. A graphical representation of the N_α EFG tensor reflecting the axial symmetry is provided in Figure 7. The figure shows a polar plot of the magnitude of the electric field gradient parallel to the direction of the electric field,[40] with the different colors (shadings) and radial extension of the surface indicating the signs and relative magnitudes of the principal components as well as the orientation of the tensor relative to the molecular frame.

A decomposition of the calculated V_{33} of free azide and of complex **3** into contributions from different LMOs is provided in Table 7. Full EFG analysis data for all complexes can be found in Tables S6−S8 of the SI. Complex **3** is representative of the set of azido complexes. Note that electronic and nuclear contributions to the EFG are both absorbed in the LMO analysis, as described in ref 40. We first discuss the EFG for N_α in free azide. The two π LPs centered on N_α contribute strongest to the overall positive V_{33}. In a symmetric environment where the EFG vanishes, there would be a perfect cancellation between the positive contributions from the π LPs and negative contributions from the σ bond and the σ LP. However, the doubly occupied N_α σ LP is s-rich, i.e., the s character of 71% is much larger than the idealized 50% expected for a sp hybridization (Table 5). Since s orbitals do not contribute to the EFG on the atom where they are centered, the low p character of the σ LP creates a rather small contribution to the N_α EFG. The N_α hybrid forming σ (N_α−N_β) is p-rich instead (70%). However, electron density from σ (N_α−N_β) is shared with the neighbor atom. The combined negative σ contributions to the N_α EFG cannot balance the large positive contributions from the π LPs (of pure p character) despite the significant delocalization of the latter over all three nitrogen atoms. In the EFG analysis for N_γ, the contribution from σ (N_β−N_γ) to the N_γ EFG is the same as the contribution from σ (N_α−N_β) to the N_α EFG. This reflects the symmetry in the σ bonding orbitals of the NBO-derived Lewis structure. For the π orbitals, the LMO analyses of the N_α and N_γ EFGs are not completely equivalent (for reasons discussed above), but the same physical picture emerges for N_γ: The negative EFG created by electron density in the σ bond (p-rich at N_γ but shared with N_β) and the s-rich σ LP cannot compensate for the positive EFG created by electron density from the π (N_β−N_γ) bonds (which includes the 3c4e contributions).

Table 7. LMO Analysis of V_{33} for Free Azide (N_3^-) and the Azido Ligands of Complex 3 (*ttt*-[$Pt(N_3)_2(OH)_2(NH_3)_2$])[a]

	azide, N_3^-			complex **3**		
LMO type	N_α	N_β	N_γ	N_α	N_β	N_γ
core N_α	0.14	−0.13	0.08	0.05	−0.23	0.01
core N_β	−0.22	0.27	−0.22	−0.26	0.08	0.18
core N_γ	0.08	−0.13	0.14	−0.01	−0.30	−0.02
π_x (N_β−N_γ)	0.02	1.13	1.13	−0.06	1.06	1.24
π_y (N_β−N_γ)	0.02	1.13	1.13	−0.08	0.57	−1.87
π_x LP N_α	1.52	0.43	0.42	1.58	0.19	0.33
π_y LP N_α	1.52	0.43	0.42	0.28	0.01	−0.27
σ LP N_α	−0.92	0.02	0.07	−0.09	−0.12	−0.11
σ LP N_γ	0.07	0.02	−0.92	−0.02	−0.14	0.57
σ (N_α−N_β)	−1.79	−1.66	−0.02	−1.47	−1.58	0.06
σ (N_β−N_γ)	−0.02	−1.66	−1.79	−0.09	−1.38	0.95
core Pt				0.17	0.58	−0.27
Pt LP				0.02	0.05	−0.02
trans total				0.26	0.40	−0.18
other BD				0.20	0.33	−0.09
other LP				0.14	0.21	−0.08
other CR				0.09	0.14	−0.04
∑ analysis	0.44	−0.14	0.44	0.70	−0.12	0.38
total calcd	0.44	−0.15	0.44	0.71	−0.12	0.38

[a]All values in au. Other BD = bonding LMOs centered elsewhere (N−C, Pt−NPy, etc.). Other LP = lone pair LMOs not centered on azide or Pt. Other CR = core orbital contributions. For a classification of the azide centered orbitals see Figures 5 and 6.

For N_β, the orbitals forming the σ bond LMOs with N_α and N_γ, respectively, are almost pure sp hybrids (51% p character). The corresponding contributions from σ (N_α−N_β) and σ (N_β−N_γ) to the N_β EFG are seen to be equivalent. An atomic sp hybrid model with evenly shared two-center σ and π bonds, assigning one electron from each of four orbitals to N_β, would yield relative EFGs of −1 from the two sp hybrids and +1 from the two p_π orbitals,[40] resulting in a vanishing EFG tensor. There is indeed a near perfect cancellation between the negative EFG contributions from the σ (N_α−N_β) and σ (N_β−N_γ) LMOs on the one hand and the positive contributions from all π LMOs on the other hand. The balance is slightly tilted toward the negative σ contributions because 56% of the density of the corresponding LMOs is associated with N_β hybrids (i.e., the density from the σ bonds is slightly more localized on N_β). The result is a negative small EFG for N_β. In the Pt complexes, this leads to weakly broadened NMR signals for the $^{14}N_\beta$ nuclei.

For complex **3**, the plots of the EFG tensors in Figure 7 and the data collected in Tables 6 and 7 show that the local symmetry of the bonding environment changes the N_α and N_γ asymmetry parameters significantly. The N_α V_{33} principal axis is approximately parallel to the N_3 axis but tilted toward the Pt center. The formation of the dative bond between azide and Pt reduces the negative V_{33} contribution from the N_α σ LP orbital significantly. The full LMO data in Tables S6−S8 of the SI show that this trend is seen across the whole set of complexes. Naively, the situation may be considered as qualitatively similar to what happens to the EFG from pyridine and amine nitrogen LP orbitals when going from free ligands to the ligand in a complex. However, for azide it is not the s-rich σ LP at N_α that forms the dative bond but rather the π_y LP (Figure 6). The

dx.doi.org/10.1021/ja3040762 | J. Am. Chem. Soc. 2012, 134, 13374−13385

corresponding change in the N_α EFG from this orbital, relative to free azide, has the expected sign: Electron density loss in this orbital reduces its *positive* contribution to the N_α EFG. Along with the formation of the ligand–metal bond occurs a p_y/p_z rehybridization in both the π_y and the σ N_α LP, as discussed in Section 3.3, i.e., mixing of local σ and π symmetry as far as the azide moiety is concerned. With regard to an EFG component in the direction of the azide axis, electron density from these two atomic orbital contributes with opposite sign (p_z:negative, p_y:positive). For the N_α π_y LP the effect is particularly large because the rehybridization *and* the density loss due to the dative bond formation reduce the EFG from this LMO relative to free azide. For the σ LP, practically all of change from its EFG contribution must be attributed to the decrease of p_z and the increase of p_y in this orbital.

The overall *negative* EFG change from the σ and π_y LPs at N_α relative to free azide is overpowered by positive EFG contributions from (i) the trans ligand (showing that delocalized bonding across the Pt center plays a significant role), (ii) from other bonding, LP, and (to a lesser degree) core orbitals in spatial proximity to the azide moiety ('other BD', 'other LP', 'other CR' in Table 7), and (iii) a less negative σ (N_α–N_β) EFG contribution in the complex. The latter effect is a simple consequence of the direction of the bond and the V_{33} principal tensor axis not coinciding in the complex (in free azide they are parallel). The final outcome, namely an increase in the N_α EFG relative to free azide, is therefore caused by a rather complex interplay of changes 'internal' to the azido ligand, each of which has a simple explanation, along with large 'external' influences, such as positive field gradient contributions from the trans ligand. The LMO analysis of the EFG provides some insight into these various trends.

The field gradient tensor at N_γ undergoes similarly dramatic changes. Most notable is the sign change from π_y (N_β–N_γ). However, the EFG tensor plots in Figure 7 show that the principal axis associated with V_{33} is not anymore (approximately) parallel to the azide axis, but rather it lies in the N_γ–N_α–Pt plane, i.e., the y–z plane of the coordinate system in Figure 7, approximately perpendicular to z. Based on the atomic hybrid orbital model put forward in ref 40, the negative EFG contribution of π_y (N_β–N_γ) at N_γ is a trivial consequence of the rotation of the V_{33} principal axis. Based on the same model, one would also expect a significantly smaller, and positive, contribution from π_x (N_β–N_γ). The LMO analysis indeed confirms this prediction.

3.5. NMR Shielding Analysis. First, we discuss the particularly large chemical shifts (low magnetic shieldings) of N_β. Due to the cylindrical symmetry, for all nitrogens in free azide tensor components $\sigma_\parallel$ parallel to the molecular axis are negligible (in nonrelativistic calculations they would vanish identically). The corresponding data are provided in Table 8. Even with a 5° bend, as it is found for the azido ligands in the Pt complexes, the $\sigma_\parallel$ tensor components do not deviate much from zero. The difference between the central and the terminal nitrogens lies in $\sigma_\perp$, the tensor components perpendicular to the N_3 axis. For N_β, the negative paramagnetic tensor components are significantly larger in magnitude. We performed a shielding analysis in terms of the canonical molecular orbitals (MOs) and applied an 'orbital rotation model' for the nitrogen 2p orbitals.[58−61] The different shielding of N_β can be traced back to contributions from two occupied σ MOs shown in Figure 8. A magnetic field perpendicular to the molecular axis can be thought of as rotating the 2p components

Table 8. Calculated Paramagnetic(σ^p) and Diamagnetic (σ^d) Shielding of a Linear Azide and a Fictitious Azide Bent by 5° [a]

		$\sigma^d_\parallel$	$\sigma^d_\perp$	$\sigma^p_\parallel$	$\sigma^p_\perp$	σ_{iso}
azide	N_α	347.7	325.2	1.3	−279.9	146.6
	N_β	353.9	297.1	2.1	−493.0	−12.0
	N_γ	347.7	325.2	1.3	−279.9	146.6
azide(5° bent)	N_α	347.7	325.2	1.5	−281.2	145.7
	N_β	353.8	297.1	1.8	−493.2	−12.2
	N_γ	347.7	325.2	1.5	−281.3	145.7

[a]Tensor components perpendicular (⊥) and parallel (∥) to the molecular axis. See Table 2 for computational details. σ^p includes SO terms.

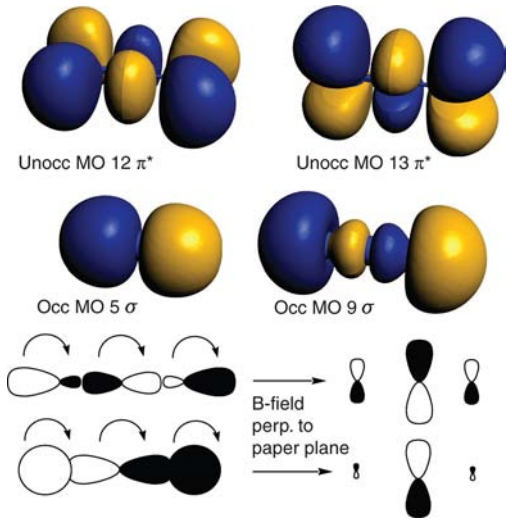

Figure 8. Selected canonical MOs of free azide. The symbolic representation of the two occupied σ orbitals illustrates qualitatively how the action of a magnetic field (**B**) perpendicular to the paper plane rotates the atomic p orbitals by 90°. The action of **B** on s-components in the atomic hybrids vanishes. The resulting magnetic-field perturbed orbitals can effectively overlap with low-energy π * MOs, in particular for the central nitrogen N_β, rationalizing the large paramagnetic $\sigma_\perp$ tensor components for this nucleus.

in the atomic hybrids forming the MOs by 90°. As shown in Figure 8, the resulting functions overlap with one of the low-lying unoccupied π^* orbitals; in particular around N_β. The amount of overlap quantifies the contribution from these occupied–unoccupied MO pairs to the paramagnetic component in $\sigma_\perp$, and it is seen to be significantly stronger for the central nitrogen. A numerical analysis of the shielding tensors components in terms of canonical MOs of azide (not shown) numerically confirmed this qualitative explanation: the combined contributions from MOs 5 and 9 to $\sigma^p_\perp$ were about 150 ppm more negative for N_β compared to the terminal nitrogens. As a result, the isotropic shielding for N_β is particularly small, and the chemical shift is large and positive. The large paramagnetic deshielding for N_β and the much lesser deshielding for N_α and N_γ can further be traced back to features of the bonding in azide already discussed in Sections 3.3 and 3.4, namely the s-rich character of the N_α, N_γ σ LP orbitals and the p-rich character of the σ bonds with N_β (which is reflected in the occupied canonical MOs in Figure 8). The delocalized π bonding also plays a role in the sense that it influences the p coefficients in the π^* MOs.

dx.doi.org/10.1021/ja3040762 | J. Am. Chem. Soc. 2012, 134, 13374–13385

Table 9. LMO Analysis of the Isotropic Nitrogen Shielding in Free Azide and in Complex 3 (*ttt*-[$Pt(N_3)_2(OH)_2(NH_3)$])[a]

	azide, N_3^-			complex 3		
LMO type	N_α	N_β	N_γ	N_α	N_β	N_γ
core N_α	241.1			241.2	−2.9	−0.6
core N_β		240.9			238.6	
core N_γ			241.1		0.3	241.2
π_x LP N_α	16.8	3.7	9.0	−34.4	−2.7	−23.6
π_y LP N_α	16.7	3.7	8.9	−361.2	−22.9	4.2
π_x (N_β–N_γ)	−0.9	16.3	6.9	−6.0	22.6	−15.5
π_y (N_β–N_γ)	−0.9	16.4	7.0	12.4	−18.6	30.8
σ LP N_α	−31.6	−32.2	−7.9	354.3	16.7	2.7
σ LP N_γ	−7.9	−32.2	−31.6	−2.8	−34.8	−84.4
σ (N_α–N_β)	−71.6	−114.4	−15.1	−66.1	−84.3	−20.1
σ (N_β–N_γ)	−15.1	−114.4	−71.6	−10.6	−144.9	−100.6
unocc[b] (SO)		0.3		45.3	21.3	7.1
core Pt				−2.9	0.5	0.5
Pt LP				−6.2	−9.6	−1.0
total trans				−7.4	6.5	1.0
others total				−9.1	2.4	−4.6
$\sum$ analysis	146.6	−11.9	146.6	146.5	−11.9	37.1
total calcd	146.6	−12.0	146.6	145.3	−13.3	37.4

[a]Contributions significantly smaller than about 1% of the total shielding not included. [b]Contributions from SO coupling in the SO-ZORA NMR calculation.

In terms of the number of formal single and double bonds, the electronic environment of N_β is somewhat similar to that of the central carbon in allene ($H_2C{=}C{=}CH_2$) which also has a particularly strongly negative $\sigma_\perp$ for the central versus the terminal carbons. The allene case has been explained previously with an 'orbital rotation model' similar to that of Figure 8.[61] However, allene differs from azide in that there is also a strong paramagnetic contribution in $\sigma_\parallel$ of the central carbon due to the lack of cylindrical symmetry of the electron density in the C=C=C moiety. For azide, the presence of actual (free linear azide) or approximate cylindrical symmetry (bent azide) suppresses $\sigma_\parallel^p$.

Table 9 provides data from a LMO analysis of the nitrogen nuclear shielding constants for free azide and for complex **3** as a representative of the set of azido Pt systems. The analysis was performed within SO ZORA NMR calculations using an 'external' set of scalar relativistic LMOs, as described in ref 41. The same set of scalar LMOs was used for the EFG analysis of Section 3.4. SO effects changing the ground-state electron density relative to a spin-free calculation show up in the shielding analysis in the form of contributions from unoccupied (unocc) external LMOs. For free azide which has no heavy atoms, these contributions are negligible. For the Pt complex, the contributions from unocc LMOs nicely show an increased shielding, in particular for N_α (45 ppm), due to SO effects. Due to the strong electron delocalization in the azide moiety, these effects are also significant for N_β (21 ppm) and even reach 7 ppm for N_γ . The strongly increased shielding of N_α covalently bound to Pt is a particularly nice example for a SO-induced heavy atom effect on a light atom NMR shielding (HALA).[62]

For brevity, the analysis has been carried out for the isotropic shielding for each azide nucleus instead of each shielding tensor component separately. As expected, the nitrogen core orbitals (1s) determine the bulk of the positive diamagnetic shielding term σ^d. For free azide, negative contributions to the paramagnetic shielding σ^p (plus SO terms related to SO induced mixing of orbitals within the occupied set) show up in contributions predominantly from the σ bond and LP LMOs. As discussed above for N_β, magnetic coupling of occupied σ with low-lying unoccupied π^* orbitals by the external field perturbation perpendicular to the N_3 axis creates large paramagnetic deshielding contributions from occupied σ orbitals. The isotropic shielding contributions from occupied π orbitals centered on the nucleus of interest are seen to be positive.

The analysis shows significant changes in the LMO shielding contributions upon binding of azide to the metal. For N_β, the net effect is rather small, although this is partially a cancellation between changes due to complexation and the 21 ppm SO shielding induced by the nearby Pt center. Since there is already a simple explanation for why the N_β shielding in free azide is so much more negative than for the other nitrogens, we focus here on the difference between N_α and N_γ in the complexes.

In Section 3.3 it has been shown that the σ and π_y LPs at N_α undergo a rehybridization when the N_α–Pt dative bond is formed (with π_y being the donor orbital) and that the π bonding in the azido ligand is more localized than in free azide. The shielding analysis of Table 9 shows that the rehybridization has a strong impact on the N_α shielding contributions from these two orbitals. However, when considering the sum of the π_y and σ LPs at N_α there is little change, overall, upon complexation. A more significant change originates from the π_x LP. This orbital becomes more localized upon complex formation (67% N_α in free azide versus 73% in **3**). Its N_α shielding contribution changes from +17 to −34 ppm. This effect is largely counter-balanced by the SO shielding effect from the heavy metal (unocc contributions). Thus, this HALA SO effect masks changes driven by chemical bonding in the N_α shielding when the complex is formed. In the end, the N_α shielding is almost the same as in free azide. This situation therefore represents an interesting case of a *hidden heavy-atom effect* in NMR spectroscopy (in contrast to cases where the SO mechanism is simply not significant).[25]

dx.doi.org/10.1021/ja3040762 | J. Am. Chem. Soc. 2012, 134, 13374−13385

In comparison, the N_γ shielding affords a much weaker Pt SO effect. Moreover, the paramagnetic shielding contributions from N_γ-centered σ LMOs become significantly more negative in the complex. This can be explained by the increased azide N_β–N_γ π bonding character in the Pt complex (see the WBIs in Table 5). As a consequence, the occupied σ orbitals couple magnetically more effectively with N_γ -centered π^* orbitals, leading to a stronger paramagnetic deshielding of N_γ.

The large difference in the N_α and N_γ chemical shifts in the azido complexes are then explained as follows: Relative to free azide, losses in magnetic shielding at N_α upon formation of the dative bond with Pt are compensated by a sizable increased N_α shielding from SO coupling at Pt (a HALA effect). The N_γ shielding is much weaker than the N_α shielding because of (i) the lack of a large SO effect from Pt and (ii) an increased paramagnetic deshielding due to the more localized N_β–N_γ π–bonds.

4. SUMMARY AND OUTLOOK

Platinum complexes with azido ligands exhibit very interesting trends in nitrogen NMR spectra. We have shown that the p-rich σ bonding and the delocalized π bonding in azide, along with changes in the azide electronic structure upon the formation of dative N–Pt covalent bonds, can be linked directly to the observed NMR trends. The direct correspondence between the chemical bonding in the azido ligand and observed NMR trends has been established with the help of an analysis of the results of first-principles theoretical calculations in terms of localized molecular orbitals (LMOs). The LMOs represent quantum mechanical analogs of Lewis electron pair bonds and LPs. For the isolated azide system, a shielding analysis in terms of regular (canonical) MOs has also been preformed in order to uncover the reason for the particularly high N_β chemical shifts in the azido complexes. Overall, the relativistic DFT calculations yielded good agreement with experimental data for ^{195}Pt, and $^{14/15}$N chemical shifts as well as Pt–N *J*-coupling constants. The LMO analysis provides a chemically meaningful and intuitive breakdown of the results. The observed trends are a consequence of (i) the delocalized π bonding in free azide versus a partial bond localization in the azide ligand, (ii) the high 2p character of the N_α–N_β and N_β–N_γ σ bonds, (iii) the high p character of the N_α–Pt bond, and (iv) a strong shielding of N_α induced by SO coupling at Pt, which compensates the electron density loss due to the N_α–Pt bond formation.

The calculated *J*-coupling constants and the Pt chemical shifts would likely benefit from a computational model based on explicit solvation at the quantum chemical level and a treatment of the solvent shell by MD. For a detailed analysis a carefully benchmarked static approach using a continuum solvent model, if suitable, is clearly preferred because otherwise the analysis would have to be averaged along a MD trajectory. We have recently performed an MD averaged LMO analysis for Hg–C *J*-coupling constants in (CH_3)–Hg–Cl and NC–Hg–CN, for the reason that in these systems explicit solvent effects are dominant, and a continuum model is not satisfactory.[63] However, the procedure then becomes rather laborious and time-consuming. Work is currently in progress in our laboratory to automate the procedures to an extent that they can be applied straightforwardly in a dynamic calculation.

One may ask the question the question whether the azide–metal bonding found here for Pt is typical for other azide complexes as well. Table S9 of the SI shows additional calculated data for azide complexes of metals with spin-1/2 nuclei (Cd, Hg, an additional Pt complex) and, for comparison, also a four-coordinate Pd complex with two azide ligands. Computations were performed for single-crystal X-ray diffraction geometries with metal–azide binding angles in the range of 116°–132°, and for geometries where the metal–azide binding angle has been increased to up to 150°. The metal–azide binding LMOs for the crystal structures are also shown in the SI (Figure S6). Table S9 additionally presents data for complex **3** for different geometries with Pt–azide angles of 118° (optimized), 130°, and 150°. The computations of the metal–N_α spin–spin coupling constants demonstrate a sensitivity to the angle at which azide is coordinated to the metal, which goes along with changes in the s character of the bond on the N_α side. The Hg systems are an exception because of the nearly vanishing N_α s character and the delocalization of the relevant LMO to the trans carbon ligand. The data indicate that for a series of related complexes with the same metal, structural differences and differences in the nitrogen s character of the metal-azide bond should be detectable by multinuclear NMR. The metal–N_α binding LMOs for the various complexes are qualitatively in agreement with the LMOs found for the Pt complexes studied herein. They all exhibit pronounced multicenter character due to the electron delocalization in the azide moieties. Differences in the metal–ligand bonding between these systems and its precise relation to observable NMR parameters may be an interesting subject of further studies.

■ ASSOCIATED CONTENT

Supporting Information

Additional calculated NMR data for ^{195}Pt and ^{15}N, *J*-coupling constants calculated at different levels of theory, LMO compositions and EFG LMO analysis for the N_3 moiety for complexes **1**–**5**, selected EFG tensor plots, additional *J*-coupling calculations, optimized geometries and energies for the Pt azide complexes from ADF calculations, and full ref 32. This material is available free of charge via the Internet at http://pubs.acs.org.

■ AUTHOR INFORMATION

Corresponding Author

jochena@buffalo.edu

Notes

The authors declare no competing financial interest.

■ ACKNOWLEDGMENTS

We thank Dr. N. J. Farrer and Prof. P. J. Sadler for bringing the interesting NMR spectroscopy of azide ligands in platinum compounds to our attention. The authors acknowledge financial support from the National Science Foundation (CHE 0952253) and are grateful for the continuing support by the Center for Computational Research at the University at Buffalo.

■ REFERENCES

(1) Bednarski, P. J.; Mackay, F. S.; Sadler, P. J. *Anti-Cancer Agents Med. Chem.* **2007**, *7*, 75–93.

(2) Farrer, N. J.; Woods, J. A.; Salassa, L.; Zhao, Y.; Robinson, K. S.; Clarkson, G.; Mackay, F. S.; Sadler, P. J. *Angew. Chem., Int. Ed.* **2010**, *49*, 8905–8908.

(3) Saxton, R. E.; Paiva, M. B.; Lufkin, R. B.; Castro, D. J. *Semin. Surg. Oncol.* **1995**, *11*, 283–289.

(4) Kratochwil, N. A.; Zabel, M.; Range, K.; Bednarski, P. J. *J. Med. Chem.* **1996**, *39*, 2499−2507.
(5) Oehlsen, M. E.; Qu, Y.; Farrell, N. *Inorg. Chem.* **2003**, *42*, 5498−5506.
(6) Berners-Price, S. J.; Frey, U.; Ranford, J. D.; Sadler, P. J. *J. Am. Chem. Soc.* **1993**, *115*, 8649−8659.
(7) Berners-Price, S. J.; Kuchel, P. W. *J. Inorg. Biochem.* **1990**, *38*, 327−345.
(8) Coluccia, M.; Natile, G. *Anti-Cancer Agents Med. Chem.* **2007**, *7*, 111−123.
(9) Pregosin, P. *Coord. Chem. Rev.* **1982**, *44*, 247−291.
(10) Pregosin, P. S. *Annu. Rep. NMR Spectrosc.* **1986**, *17*, 285−349.
(11) Van Beusichem, M.; Farrell, N. *Inorg. Chem.* **1992**, *31*, 634−639.
(12) MacDonald, F. M.; Sadler, P. J. *Polyhedron* **1991**, *10*, 1443−1448.
(13) Fontes, A. P. S.; Oskarsson, A.; Lövqvist, K.; Farrell, N. *Inorg. Chem.* **2001**, *40*, 1745−1750.
(14) Albrecht, M.; Rodríguez, G.; Schoenmaker, J.; van Koten, G. *Org. Lett.* **2000**, *2*, 3461−3464.
(15) Still, B. M.; Kumar, P. G. A.; Aldrich-Wright, J. R.; Price, W. S. *Chem. Soc. Rev.* **2007**, *36*, 665−686.
(16) Truflandier, L. A.; Autschbach, J. *J. Am. Chem. Soc.* **2010**, *132*, 3472−3483.
(17) Truflandier, L. A.; Sutter, K.; Autschbach, J. *Inorg. Chem.* **2011**, *50*, 1723−1732.
(18) Sutter, K.; Truflandier, L. A.; Autschbach, J. *ChemPhysChem* **2011**, *12*, 1448−1455.
(19) Autschbach, J.; Ziegler, T. *J. Am. Chem. Soc.* **2001**, *123*, 3341−3349.
(20) Bühl, M.; Mauschick, F. T.; Terstegen, F.; Wrackmeyer, B. *Angew. Chem., Int. Ed.* **2002**, *41*, 2312−2315.
(21) Sterzel, M.; Autschbach, J. *Inorg. Chem.* **2006**, *45*, 3316−3324.
(22) Farrer, N. J.; Gierth, P.; Sadler, P. J. *Chem.—Eur. J.* **2011**, *17*, 12059−12066.
(23) Wrackmeyer, B.; Kupce, E.; Köster, R.; Seidel, G. *Magn. Reson. Chem.* **1992**, *30*, 393−397.
(24) O'Dell, L.; Schurko, R.; Harris, K.; Autschbach, J.; Ratcliffe, C. *J. Am. Chem. Soc.* **2011**, *133*, 527−546.
(25) Autschbach, J.; Zheng, S. *Annu. Rep. NMR Spectrosc.* **2009**, *67*, 1−95.
(26) Gilbert, T. M.; Ziegler, T. *J. Phys. Chem. A* **1999**, *103*, 7535−7543.
(27) Autschbach, J.; Le Guennic, B. *Chem.—Eur. J.* **2004**, *10*, 2581−2589.
(28) Le Guennic, B.; Matsumoto, K.; Autschbach, J. *Magn. Reson. Chem.* **2004**, *42*, S99−S116.
(29) Koch, K. R.; Burger, M. R.; Kramer, J.; Westra, A. N. *Dalton Trans.* **2006**, 3277−3284.
(30) Moncho, S.; Autschbach, J. *J. Chem. Theory Comput.* **2010**, *6*, 223−234.
(31) Burger, M. R.; Kramer, J.; Chermette, H.; Koch, K. R. *Magn. Reson. Chem.* **2010**, *48*, S38−S47.
(32) Baerends, E. J.; et al. *Amsterdam Density Functional (ADF)*, Developers' version, SCM; Theoretical Chemistry; Vrije Universiteit: Amsterdam, The Netherlands, 2012.
(33) van Lenthe, E.; Baerends, E. J.; Snijders, J. G. *J. Chem. Phys.* **1993**, *99*, 4597−4610.
(34) Wolff, S. K.; Ziegler, T.; van Lenthe, E.; Baerends, E. J. *J. Chem. Phys.* **1999**, *110*, 7689−7698.
(35) Autschbach, J.; Zurek, E. *J. Phys. Chem. A* **2003**, *107*, 4967−4972.
(36) Krykunov, M.; Ziegler, T.; van Lenthe, E. *J. Phys. Chem. A* **2009**, *113*, 11495−11500.
(37) Autschbach, J.; Ziegler, T. *J. Chem. Phys.* **2000**, *113*, 9410−9418.
(38) Autschbach, J. *J. Chem. Phys.* **2008**, *129*, 094105−9; Erratum ibid. 130 (2009), 209901.
(39) Harris, R. K.; Becker, E. D.; Cabral de Menezes, S. M.; Goodfellow, R.; Granger, P. *Pure Appl. Chem.* **2001**, *73*, 1795−1818.
(40) Autschbach, J.; Zheng, S.; Schurko, R. W. *Concepts Magn. Reson. A* **2010**, *36A*, 84−126.
(41) Autschbach, J. *J. Chem. Phys.* **2008**, *128*, 164112−11.
(42) Autschbach, J.; Zheng, S. *Magn. Reson. Chem.* **2008**, *46*, S48−S55.
(43) Glendening, E. D.; Badenhoop, J. K.; Reed, A. E.; Carpenter, J. E.; Bohmann, J. A.; Morales, C. M.; Weinhold, F. *NBO 5.0*, Theoretical chemistry institute; University of Wisconsin: Madison, WI, 2001; http://www.chem.wisc.edu/~nbo5.
(44) Weinhold, F. Natural bond orbital methods. In *Encyclopedia of computational chemistry*; von Ragué Schleyer, P., Ed.; John Wiley & Sons: Chichester, U.K., 1998, pp 1792−1811.
(45) Hammer, B.; Hansen, L. B.; Nørskov, J. K. *Phys. Rev. B* **1999**, *59*, 7413.
(46) Truflandier, L. A.; Brendler, E.; Wagler, J.; Autschbach, J. *Angew. Chem., Int. Ed.* **2011**, *50*, 255−259.
(47) Pye, C. C.; Ziegler, T. *Theor. Chem. Acc.* **1999**, *101*, 396−408.
(48) Bondi, A. *J. Phys. Chem.* **1964**, *68*, 441−451.
(49) Marenich, A. V.; Cramer, C. J.; Truhlar, D. G. *J. Phys. Chem. B* **2009**, *113*, 6378−6396.
(50) Polak, M.; Gruebele, M.; Saykally, R. J. *J. Am. Chem. Soc.* **1987**, *109*, 2884−2887.
(51) Brazier, C. R.; Bernath, P. F.; Burkholder, J. B.; Howard, C. J. *J. Chem. Phys.* **1988**, *89*, 1762−1767.
(52) Pregosin, P. S.; Streit, H.; Venanzi, L. M. *Inorg. Chim. Acta* **1980**, *38*, 237−242.
(53) Autschbach, J. The calculation of NMR parameters in transition metal complexes. In *Principles and Applications of Density Functional Theory in Inorganic Chemistry I*; Kaltsoyannis, N., McGrady, J. E., Eds.; Springer: Heidelberg, Germany, 2004; Vol. *112*, pp 1−48.
(54) Müller, P.; Schröder, B.; Parkinson, J. A.; Kratochwil, N. A.; Coxall, R. A.; Parkin, A.; Parsons, S.; Sadler, P. J. *Angew. Chem., Int. Ed.* **2003**, *42*, 335−339.
(55) Autschbach, J.; Le Guennic, B. *J. Chem. Educ.* **2007**, *84*, 156−171.
(56) Pyykkö, P. *Mol. Phys.* **2008**, *106*, 1965−1974.
(57) Townes, C. H.; Dailey, B. P. *J. Chem. Phys.* **1949**, *17*, 782−796.
(58) Cornwell, C. D. *J. Chem. Phys.* **1966**, *44*, 874−880.
(59) Jameson, C. J.; Gutowsky, H. S. *J. Chem. Phys.* **1964**, *40*, 1714−1724.
(60) Grutzner, J. B. Chemical shift theory. Orbital symmetry and charge effects on chemical shifts. In *Recent advances in organic NMR spectroscopy*; Norell Press: Landisville, NJ, 1987, pp 17−42.
(61) Wiberg, K. B.; Hammer, J. D.; Zilm, K. W.; Cheeseman, J. R. *J. Org. Chem.* **1999**, *64*, 6394−6400.
(62) Edlund, U.; Lejon, T.; Pyykkö, P.; Venkatachalam, T. K.; Buncel, E. *J. Am. Chem. Soc.* **1987**, *109*, 5982−5985.
(63) Zheng, S.; Autschbach, J. *Chem.—Eur. J.* **2011**, *17*, 161−173.